Radio galaxies of intermediate radio luminosity: a discussion of the radio properties of B2 0836+29, B2 0844+31 and B2 1521+28

A. Capetti¹, R. Fanti^{2,3}, and P. Parma²

¹ Space Telescope Science Institute, 3700 San Martin Drive Baltimore, MD 21218 USA

² Istituto di Radioastronomia CNR, Via Gobetti 101, I-40129 Bologna, Italy

Received 28 September 1994 / Accepted 30 November 1994

Abstract. We present total intensity and polarization data of three B2 radio galaxies with of radio luminosity in the range $P_{1.4} = 10^{24.6} - 10^{24.8} \text{ W Hz}^{-1}$, intermediate between FRI and FRII objects. The sources were observed at 6 and 20 cm in different configurations of the VLA.

We discuss the morphology, the polarization and the spectral properties of these objects and particularly of their jets. In certain aspects their behaviour is intermediate between the FRI or FRII radio galaxies, leading to the conclusion that they are transition objects between the two classes. In two of these sources depolarization and rotation measure analysis clearly display the Laing-Garrington effect. Spectral steepening in the the low brightness regions leads to an estimate of the ages of the sources. From energy arguments and from the asymmetry in the jet brightness, we estimate that velocities in the jets are of the order of 0.5c - 0.7c in the first 5 kpc and then decrease to $\lesssim 0.2c$ at ga20 kpc from the core. The jet Mach numbers are estimated in the range of 4–6.

Key words: galaxies: B2 0836+29; B2 0844+31; B2 1521+28; jets-polarization – radio continuum: galaxies

1. Introduction

The classification of radio sources in Fanaroff Riley class I (FR I) and class II (FR II) reflects a difference in radio structure and radio luminosity.

FR I radio sources have a relatively relaxed morphology with edge-darkened lobes in which the brightness gradually dies away. This class includes different types of sources such as wide doubles, edge-darkened doubles, tailed and complex sources. Jets are a common feature in these sources; they are prominent, two-sided and rapidly expanding with a magnetic field predominantly perpendicular to the jet axis. These sources generally have $P_{1.4} < 10^{25}$ W Hz⁻¹. FR II sources, often referred to as "classical doubles" have edge- brightened lobes (hot-spots) and

Send offprint requests to: P. Parma

the jets are much less prominent, one-sided, well collimated and with a magnetic field predominantely parallel to the jet axis; often knots are present. These sources are more powerful than those of the FRI class, with $P_{\rm 1.4} > 10^{25}~{\rm W\,Hz^{-1}}$.

However, this classification is rather schematic and the reality is more complex: the VLA observations at 20 cm of the B2 sample of low luminosity radio galaxies had already revealed that in the range of power $P_{1.4} = 10^{22} - 10^{25}$ W Hz⁻¹ a large variety of jet-types exists (Parma et al. 1987). More recent observations (De Ruiter et al. 1993) have confirmed the existence of "naked jets": sources with only a core plus a twin-jet, but without any lobes. On the other hand we also find double symmetric jets embedded in double lobes. An important step for a better understanding of the physical difference between FRI and FRII is to study objects with a luminosity intermediate between the two classes.

This work presents the results of the observations of three such radiogalaxies of intermediate luminosity ($P_{1.4} = 10^{24.6} - 10^{24.8} \text{ W Hz}^{-1}$). These galaxies show bright cores, one-sided jets and their linear sizes are significantly larger than the average value corresponding to their radio luminosity (see de Ruiter et al. 1990). Their properties are summarized in Table 1. In Sect. 2 we describe the observations and the data reduction procedure, while in Sects. 3, 4, 5 and 6 we present the results of the observations. In Sect. 7 we discuss some properties of these three sources.

Through out this paper we adopted $H_0 = 100 \,\mathrm{km}\,\mathrm{s}^{-1}$.

2. Observations and data reduction

VLA observations at 6, 18 and 20 cm have been obtained in different configurations. A description of the VLA and its modes of operation can be found in Napier et al. (1983).

The data at 18 and 20 cm are described in Fanti et al. (1987 and references therein). The source B2 0844+31 was reobserved at 20 cm with the C array to improve the coverage of the UV plane at the short spatial frequencies.

³ Dipartimento di Fisica, Università di Bologna, Via Irnerio 46, I-40126 Bologna, Italy

Table 1. Integral properties

	0836+29	0844+31	1521+28
R.A.	08 36 13.4	08 44 54.2	15 21 21.4
Dec.	29 01 17	31 58 14	28 48 07
Z	0.079	0.0675	0.0825
$m_{ m pg}$	14.7	15.5	15.4
$S_{20\mathrm{cm}}$ (mJy)	600	1265	602
$M_{ m pg}$	- 22.4	-21.1	- 21.7
$\log P_{20}$	24.73	24.8	24.60
L.A.S.(")	345	300	200
LLS (kpc)	331	325	232
Spectral index	0.7	0.86	0.72
L_n	2.4	1.6	1.5
kpc arcsec ⁻¹	1.2	1.0	1.2
$(S_{\rm mj}/S_{\rm ex})_n$	1.7	0.6	1.4

Notes: P_{20} is the radio power at 1.4 GHz, measured in W Hz. L_n is the ratio of the source linear size to the average size of sources of similar radio power.

Table 2a. Observations of 0836+29

Date	Frequency (MHz)	Array	Duration (min)
May 1984	1435	С	30
September 1982	1435	В	54
December 1984	1435	Α	14
December 1989	4860	D	45
August 1990	4860	В	60

Table 2b. Observations of 0844+31

Date	Frequency (MHz)	Array	Duration (min)
October 1989	1435	C	60
May 1985	1435	В	15
December 1989	4860	D	45
October 1989	4860	C	60
August 1990	4860	В	60

The observations at 6 cm were made in different configurations, selected in order to produce the same UV plane coverage as at 20 cm. For the sources 1521+28 and 0844+31 we have also obtained observations at a higher resolution (A configuration). Each source was observed for about an hour for every configuration, at the frequencies of 4835 and 4885 MHz, with a bandwidth of 50 MHz.

The parameters of the observations are given in the Tables 2a, 2b and 2c.

The flux densities were brought on the scale of Baars et al. (1987) using 3C 286 as primary flux calibrator. We observed a phase calibrator after or before every source of the program. Polarization angles were measured relative to that of 3C 286; we observed secondary calibrators on a wide range of parallactic

Table 2c. Observations of 1521+28

Date	Frequency (MHz)	Array	Duration (min)
May 1984	1435	С	10
May 1985	1435	В	24
September 1982	1435	Α	15
December 1989	4860	D	45
August 1990	4860	В	60
June 1990	4860	Α	60

angles in order to determine a good solution for the instrumental polarization calibration and we corrected the data for it. We expect that the residual error on the fractional polarization is about 0.3~%.

Post-calibration reduction was done using the National Radio Astronomy Observatory AIPS package at the VLA and at the University of Turin. The data of each observation were reduced separately; the two different frequencies of the 6 cm observations were combined and reduced as a single data set; conversely we re-analyzed the 18 and 20 cm data separately.

To improve the phase calibration and to correct the phase for instrumental and atmospheric errors, we used the selfcalibration algorithm of Schwab (1980); the CLEAN algorithm (Hogbom 1974; Clark 1980) was used to produce the model images. A few iterations, usually three, were sufficient to correct the data.

The corrected data obtained in the different configurations for each source were combined to improve the UV plane coverage. A further self-calibration was performed to correct for small displacements in the individual observations. Using different gaussian weight functions we produced maps of the Stokes parameter I, Q and U at different resolution, in order to study the different features of the sources. The relevant parameters of the maps produced are given in Tables 3 a,b,c. We display in Figs. 1, 2a,b and 3 the new low resolution maps, at 5 GHz for 0836+29 and 1521+28 and at 1.4 and 5 GHz for 0844+31. We refer to previous papers (see Fanti et al. 1987) for the other 1.4 GHz maps.

Table 3a. Maps of 0836+29

Frequency (MHz)	FWHP (arcsec)	Noise (r.m.s.) (mJy beam ⁻¹) ^a
1435	10.9	0.5 (0.07)
1435	1.5	0.12 (0.07)
4860	10.9	0.05 (0.03)
4860	3.0	0.05 (0.03)
4860	1.5	0.05 (0.03)

3. Radio cores

Each of the three sources exhibits a rather bright radio core. The radio spectrum is flat or slightly inverted between 1.4

Table 3b. Maps of 0844+31

Frequency (MHz)	FWHP (arcsec)	Noise (r.m.s.) (mJy beam ⁻¹) ^a
1435	10.6	0.1 (0.07)
1435	4.5	0.15 (0.07)
4860	10.6	0.05 (0.03)
4860	4.5	0.04 (0.03)
4860	1.4	0.03 (0.03)

Table 3c. Maps of 1521+28

Frequency (MHz)	FWHP (arcsec)	Noise (r.m.s.) (mJy beam ⁻¹) ^a
1435	10.7	0.10 (0.06)
1435	1.6	0.12 (0.06)
4860	10.7	0.05 (0.03)
4860	1.6	0.03 (0.03)
4860	0.6	0.04 (0.03)

^a Values in parentheses refer to U and Q maps.

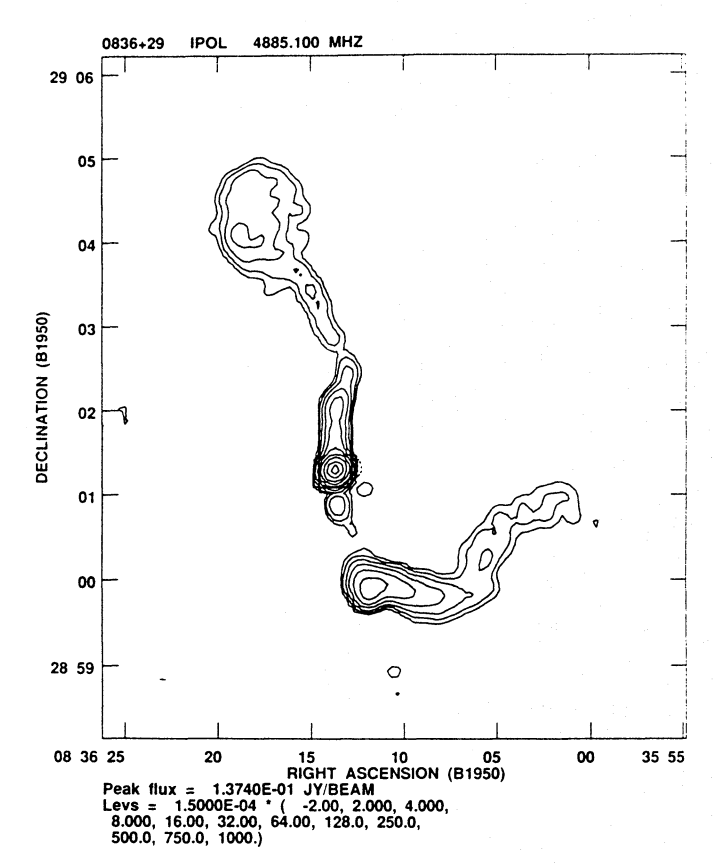


Fig. 1. Total intensity map of B2 0836+29 at 4885 MHz, with resolution of 10.9'' (FWHM)

and 4.9 GHz (using maps of similar resolution) so that we expect little contamination from the sub-arcsec jet. In the case of

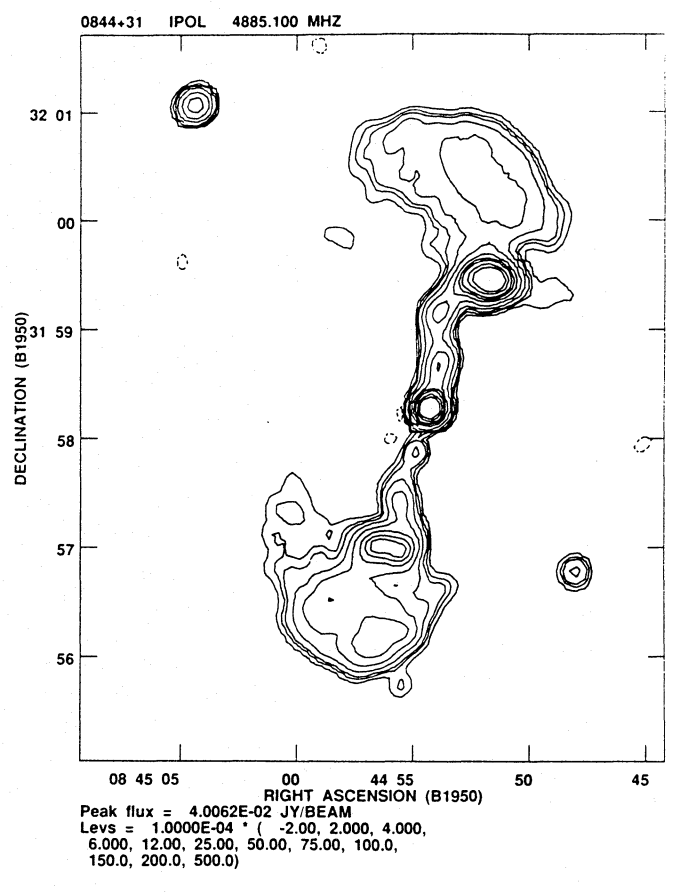


Fig. 2a. Total intensity map of B2 0844+31 at 4885 MHz, with resolution of 10.6" (FWHM)

0836+29, a VLBI map (Venturi et al. 1994) shows that the mas core accounts for > 80% of our VLA flux.

Table 4 gives the core parameters. $P_{\rm cn}$ is the ratio of the core flux to the extended flux, normalized to the average value for sources of the same total radio power (de Ruiter et al. 1990). The three radio cores all have $P_{\rm cn} > 1$.

4. The radio jets

The three sources were selected for this study because of their bright radio jets. Maps of the jets at intermediate and high resolution are shown in Figs. 4ab, 5ab and 6ab.

They exhibit the following common characteristics:

- (a) strong asymmetry in brightness;
- (b) small opening angle ($\lesssim 5 \text{ deg.}$);
- (c) different regimes of expansion;
- (d) bright knots, mainly at the beginning of the jets;
- (e) oscillations;
- (f) magnetic field aligned with the jet axis at the beginning, flipping to perpendicular at some distance from the core.

These characteristics are similar to those of jets of high luminosity FRII radio galaxies.

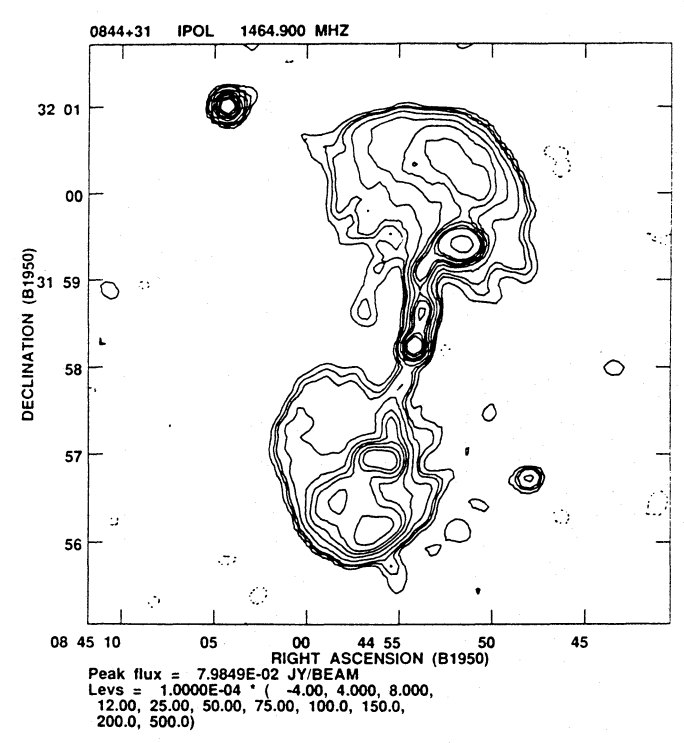


Fig. 2b. Total intensity map of B2 0844+31 at 1465 MHz, with resolution of 10.9" (FWHM)

4.1. Brightness asymmetry

In Table 5 we give the jet brightness ratio for the three sources, at various distances from the core. Sidedness parameter, $A_{\rm j}$, (defined as the average brightness ratio between the main jet and counterjet, corrected for the underlying lobe emission) is large in the first 10–15 kpc and then its reduces somewhat. The largest change is for 0844+31, where it drops from $\gtrsim 30$ at a few kpc to ~ 2 at more than 40 kpc.

4.2. Jet expansion

The jet transverse profiles are fitted with gaussian functions and the FWHM, deconvolved for the beam size, is taken as a measure of the jet transverse size.

The average opening angle of the main jets (defined as the ratio of the transverse jet size, at half jet lengths, to the distance from the core) is 5 ± 1 deg for each source. Figures 7a, 8a and 9a show the expansion of the jets, using width measures from the maps at the various resolutions. It is clear that the jets do not expand at a constant rate. Several regimes are seen where expansion is followed by recollimation. They are summarized in Table 6.

The counter-jets are too weak for measuring accurately the jet size, so that a detailed study of their expansion regimes is not possible. Roughly speaking, whenever the counter-jet transverse size is measurable with enough accuracy, it appears to be larger than that of the main jet (about 20% difference in 0836+29, and 5% for 0844+31).

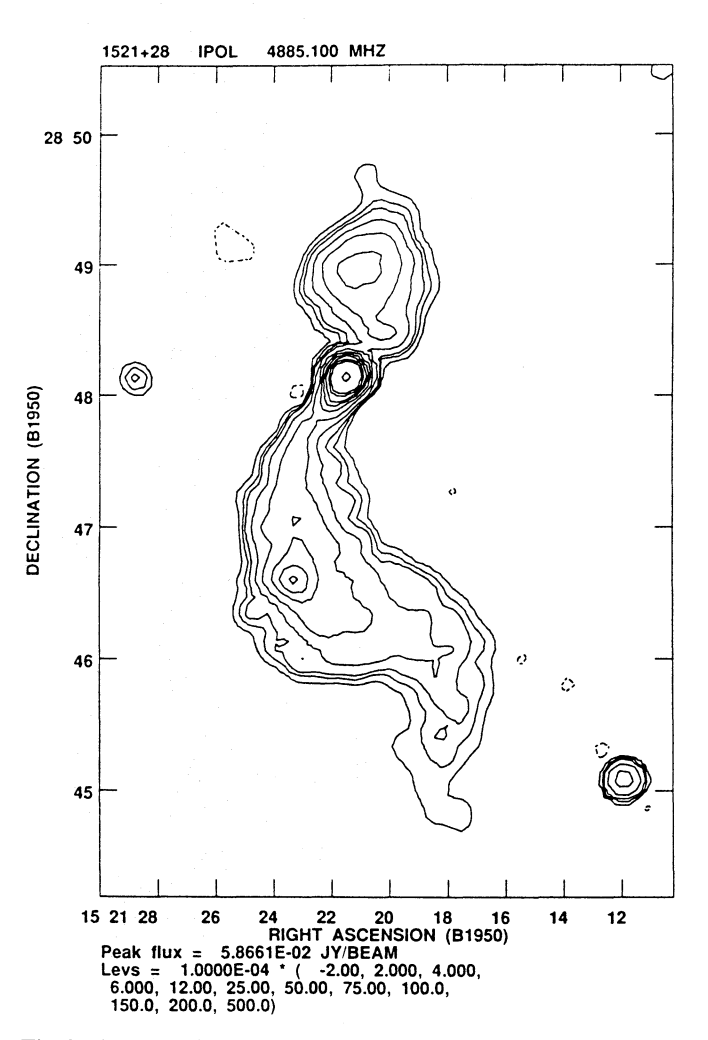


Fig. 3. Total intensity map of B2 1521+28 at 4885 MHz, with resolution of 10.7" (FWHM)

Table 4. Core properties

	0836+29	0844+31	1521+28
R.A.	08 36 13.57	08 44 54.23	15 21 21.41
Dec.	29 01 15.38	31 58 13.7	28 48 08.44
S_{6cm} (mJy)	152	40	56
$S_{20\mathrm{cm}}$ (mJy)	110	30	44
$lpha^{a}$	- 0.24	- 0.38	- 0.2
$\log P_{\rm c}$ (6 cm)	23.86	23.30	23.57
P_{cn}	10.	1.8	4.5
% Pol. (6 cm)	< 0.5	2.4	3.0
Pol. p.a. (deg)	<u>-</u>	83	60

^a α (spectral index) is defined as: $S(\nu) \sim \nu^{-\alpha}$.

4.3. Brightness distribution along the jets

Several brightness knots are seen in the jets of each source, superposed on smoother low-level emission. At the available resolutions, the knots separations, in units of jet diameter, are in the range of 7 to 2. Furthermore, it seems that the separation decreases with distance from the core. However one has the

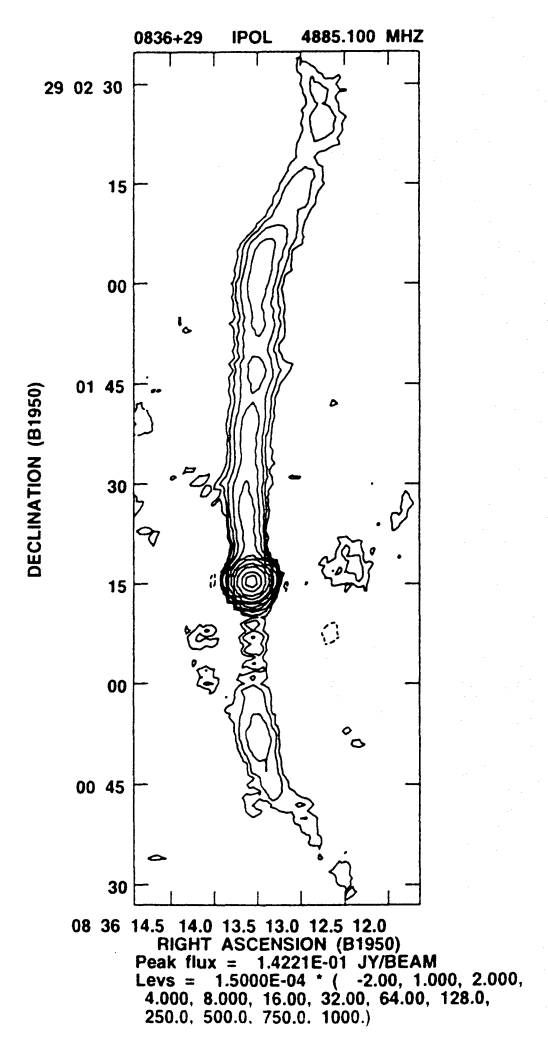


Fig. 4a. Total intensity map of the jets of B2 0836+29 at 4885 MHz, with resolution of 3.3"(FWHM)

impression that, as the resolution increases, the knots break up again in other smaller knots. Figures 7b, 8b and 9b show how the jet brightness varies with jet transverse size. The behaviour of the jet brightness as a function of the jet transverse size, $d_{\rm j}$, is clearly sub-adiabatic: fitting the brightness-size behaviour with a single power law, $d_{\rm j}^{-\delta}$, the exponent δ is found in the range 1.5–1.8, while it would be expected to be \sim 3.5 if the expansion were adiabatic and the jet had a constant speed (Fanti et al. 1982). Anyhow, a single power law is a poor fit and deviations are clearly seen.

4.4. Oscillations

The ridge lines of the jets are not straight, but show oscillations and/or large scale bends. We have produces plots of the ridge-line deviations from the average source axis. These plots (not shown here) do confirm the the oscillations visible from the contour plots.

In the case of 0844+31 both the main jet and the counter-jet show a sine wave type oscillation, with amplitude of $\sim 10''$ and

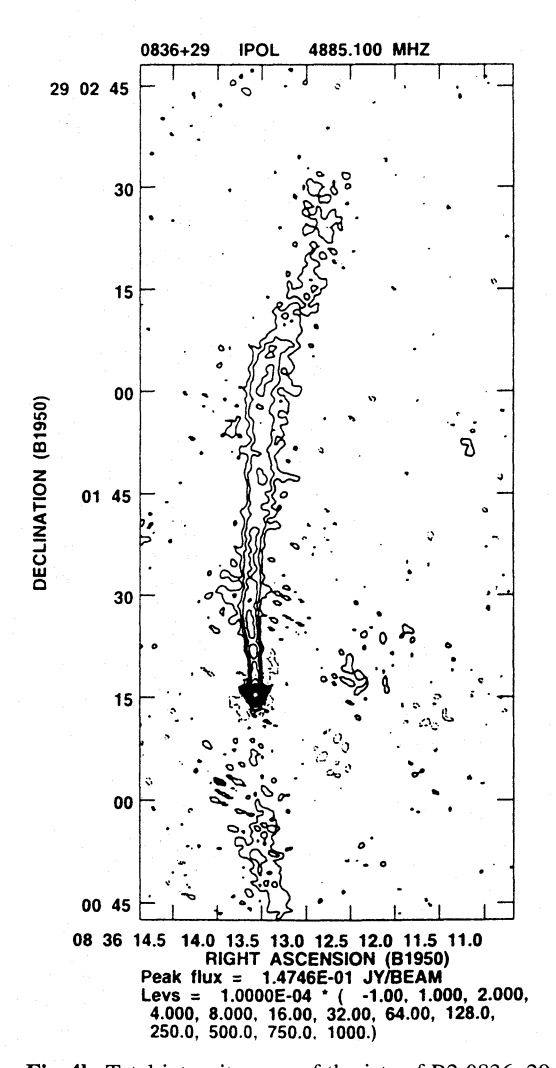


Fig. 4b. Total intensity map of the jets of B2 0836+29 at 4885 MHz, with resolution of 1.5'' (FWHM)

remarkable mirror symmetry with respect to the core and with a wavelength of $\sim 60''$ (the average wavelength/jet radius is ~ 60), corresponding roughly to the length of the two jets.

In 0836+29 a small amplitude (2") oscillation with wavelength of ~ 36 " (wavelength/jet radius ratio ~ 25) is seen in the initial bright part of the main jet. Afterwards the jet undergoes a significant bend to west followed by a counter-bend to east.

Also 1521+31 shows a small amplitude (0.5'') oscillation with wavelength $\sim 17''$ (wavelength to jet radius ~ 28) in the bright initial part of the jet, followed by a systematic counterclockwise bending.

We note that the jets become fainter and wider with increasing distance from the core and thus are more difficult to study, at a given resolution, further from the core. There is therefore some bias toward detecting longer wavelength oscillations in the outer parts of the jet and shorter wavelength oscillations in the inner parts.

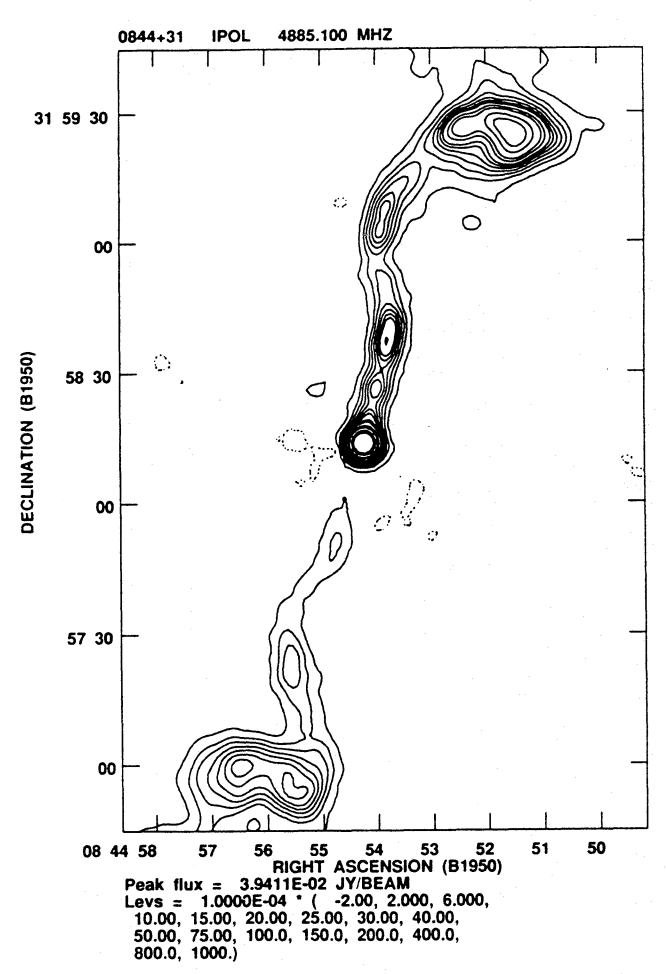


Fig. 5a. Total intensity map of the jets of B2 0844+31 at 4885 MHz, with resolution of 4.5" (FWHM)

4.5. Polarization and magnetic field direction

All three main jets are polarized at 6 cm and somewhat less at 20 cm. The best information is for 0844+31, owing to the better signal-to-noise ratio. A profile of fractional polarization along the jet ridge line is given in Fig. 10. Large fluctuations are evident. Rotation of p.a. between 20 and 6 cm is moderate in all three sources and allows us to determine the orientation of the intrinsic polarization and consequently of the magnetic field. In B2 0836+29 the magnetic field is parallel to the jet axis within the first 15 kpc; than it flips to perpendicular and maintains this orientation up to \sim 45 kpc, where, in correspondence with the beginning of the large westward bend, it flips to parallel again (Fig. 11a).

In B2 0844+31 the transition from parallel to perpendicular occurs at ~ 25 kpc. The field becomes longitudinal again in correspondence with the large bend at ~ 45 kpc from the core (Fig. 11b).

In B2 1521+28 the field is parallel to the jet axis in the first 20 kpc; beyond that the polarization is too weak to allow any estimate (Fig. 11c).

We note that the initial parallel regime of the magnetic field corresponds in all three sources to a larger asymmetry in the jet to counter-jet brightness ratio.

4.6. Spectral index along the jets

Comparison of 6 and 20 cm maps at similar resolution allows a determination of the spectral index along the jets. Variations are minor and uncertain.

In B2 0836+29 the spectral index is close to 0.6, with small oscillations, up to a distance of ~ 100 kpc, after which it steepens reaching the value of 0.9 before entering in the lobe.

In B2 0844+31 the spectral index of the main jet is mostly between 0.5 and 0.6, with some oscillations; it reaches a maximum of ~ 0.85 at about 70 kpc and than flattens again to 0.65 before entering in the lobe. In the counterjet, the spectrum is somewhat steeper, with an average value of ~ 0.7 and fluctuations from 0.5 to 1.1.

In B2 1521+38 the spectral index is 0.65 ± 0.05 up to 20 kpc from the core, than it seems to decrease slightly to a value of 0.6 at 45 kpc.

5. The hot spots

Here we give a definition of "hot spot" as in De Ruiter et al. (1990), namely brightness, at $20\,\mathrm{cm.}$, $\geq 0.6\,\mathrm{mJy\,arcsec^{-2}}$ and brightness contrast ≥ 4 with respect to the underlying lobe. We used the higher resolution maps. The properties of the hot spots are summarized in Table 8.

The source B2 0844+31 shows a hot spot in each lobe. The hot spots are remarkably anti-symmetric in shape. The brighter hot spot is found at the end of the brighter jet.

In B2 0836+29 a hot spot on the counter-jet side is found, better visible on the higher resolution map (not shown here). The hot spot of B2 1521+31 is the weakest one and it is on the main jet side. Note also that in 0844+31 the hot-spots are located in the inner parts of the lobes; in 1521+28, the hot spot is at the center of the radio lobe.

In 0844+31, the southern hot spot is significantly more depolarized than the northern one, with depolarization ratios, D, $\sim 0.45 \pm 0.1$ and $\sim 0.85 \pm 0.1$ respectively (the depolarization ratio D is defined as the ratio of the fractional polarization at 1.4 GHz over that at 4.9 GHz, computed as in Garrington et al. 1991). Their projected magnetic field exhibits a remarkable circumferential geometry (see Fig. 11b).

6. The radio lobes

6.1. Morphology

The properties of the radio lobes are summarized in Table 9.

In B2 0836+29 the two lobes are symmetric in total emission, but quite asymmetric in shape and maximum extent from the core. The southern lobe has a tail-like shape, while the northern one is roundish.

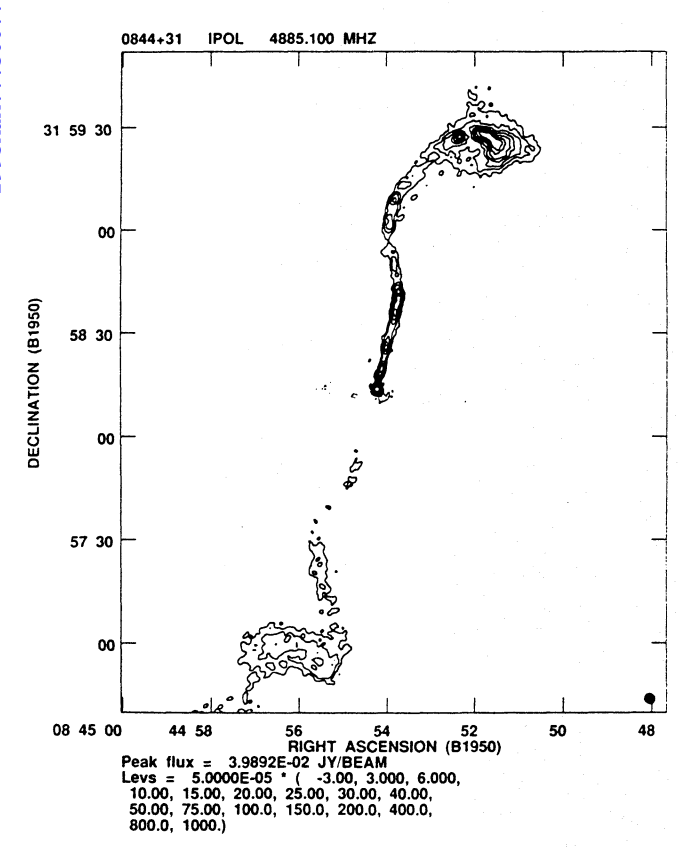


Fig. 5b. Total intensity map of the jets of B2 0844+31 at 4885 MHz, with resolution of 1.4" (FWHM)

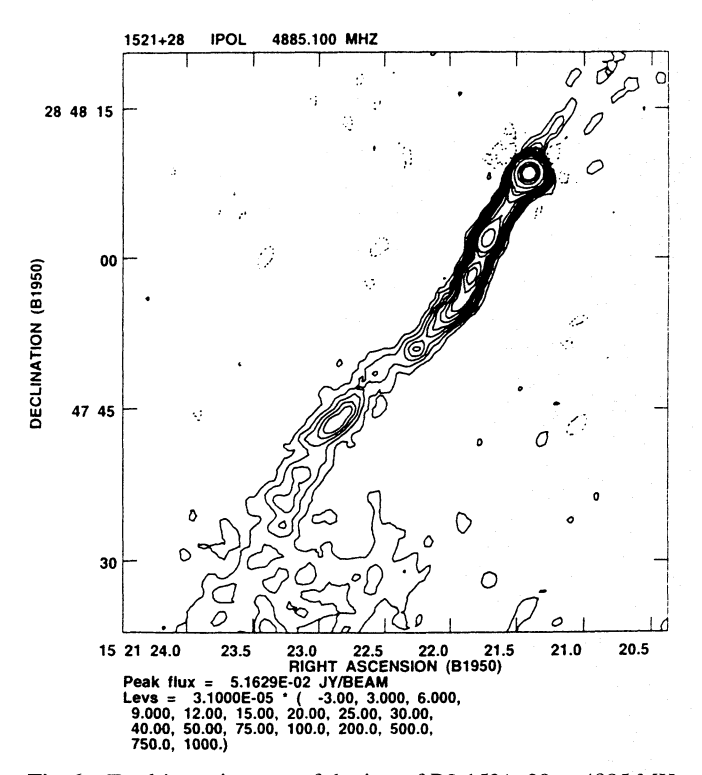


Fig. 6a. Total intensity map of the jets of B2 1521+38 at 4885 MHz, with resolution of 1.6'' (FWHM)

Table 5. Jets brightness asymmetry

Name	Distance (kpc)	$A_{\rm j}$
0836+29	0–15 15–35 35–55	≥ 5 ≥ 2.5 ≥ 5
0844+31	0–15 15–40 40–60	$>> 20$ $\sim 10-3$ ~ 2
1521+28	0– 8 8–15	> 10 ≥ 6

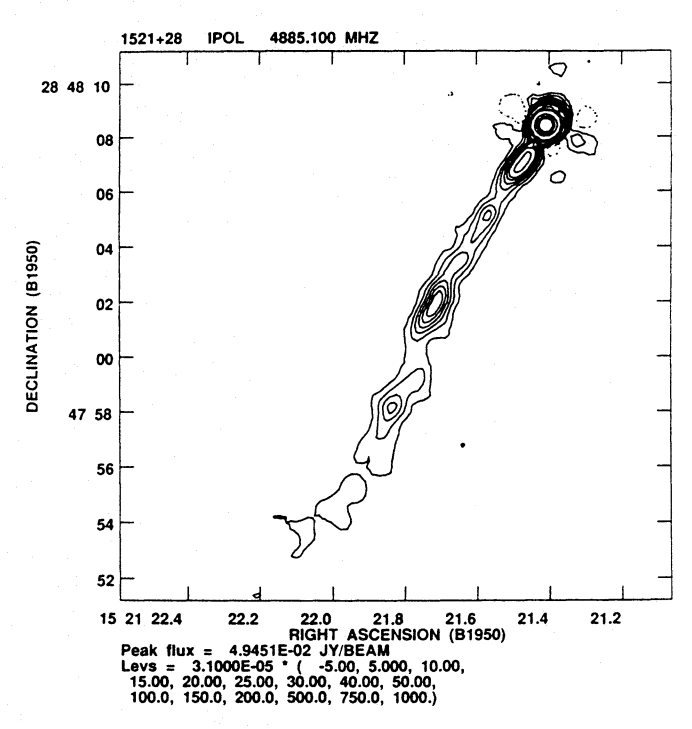


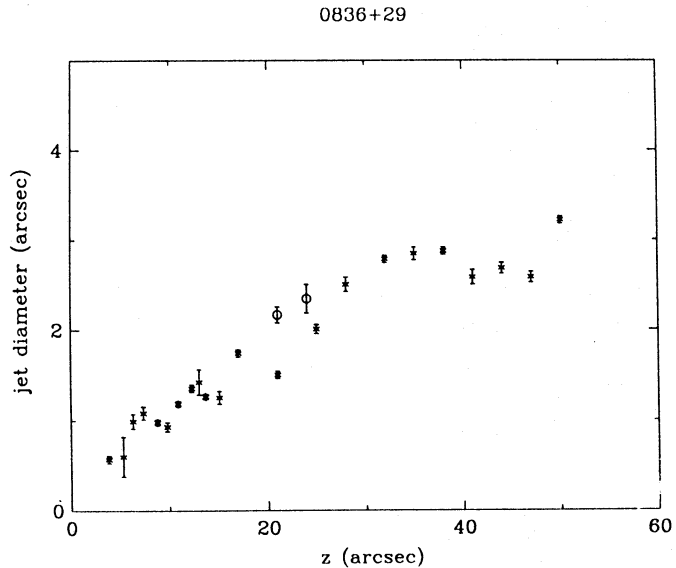
Fig. 6b. Total intensity map of the jets of B2 1521+38 at 4885 MHz, with resolution of 0.6'' (FWHM)

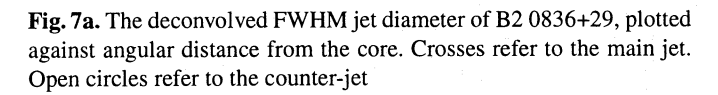
In B2 1521+28 the lobes are asymmetric both in their radio flux (ratio 1.9 to 1), maximum extension from the core (ratio 2 to 1) and shape. As for 0836+29, the lobe containing the hot spot shows a tail-like extension.

Finally 0844+31 has very symmetric lobes in flux, shape and maximum extent.

6.2. Spectral index distribution

The radio spectra within the lobes are computed using the maps at 10'' resolution. In all three sources we find significant variations of the spectral index. In 0836+29 the northern lobe has a spectral index ~ 1.1 , possibly slightly flatter at the brightness peak. On the contrary the southern, tail-shaped lobe shows a clear steepening from the hot spot (~ 0.5) to east, up to ~ 1.4 .





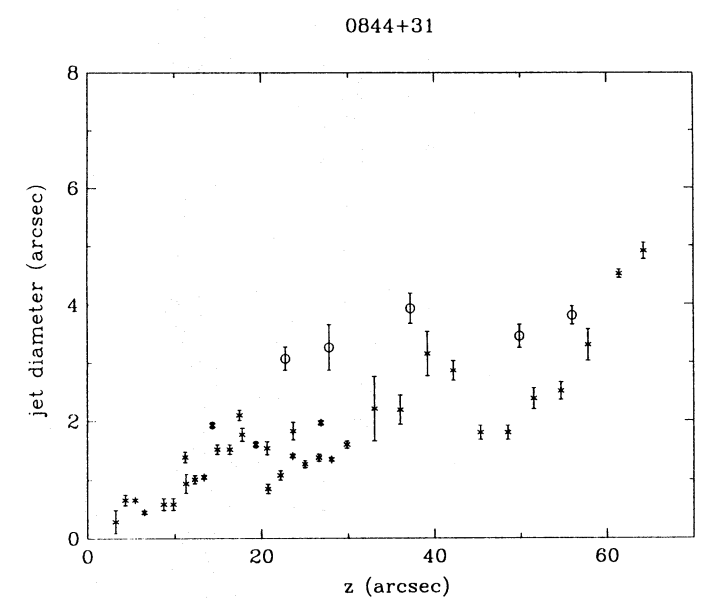


Fig. 8a. The deconvolved FWHM jet diameter of B2 0844+31, plotted against angular distance from the core. Crosses refer to the main jet. Open circles refer to the counter-jet

0844 + 31

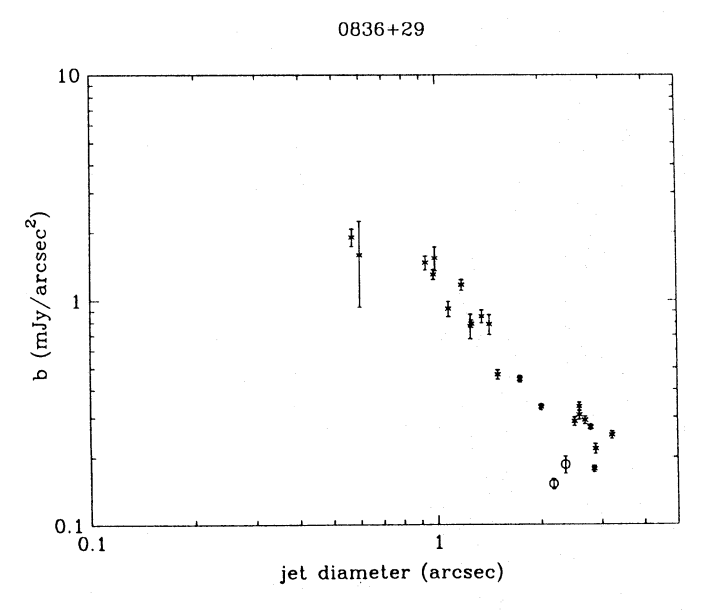


Fig. 7b. The deconvolved jet brightness of B2 0836+29, at 4885 MHz, plotted against deconvolved transverse jet size. Open circles refer to the counter-jet

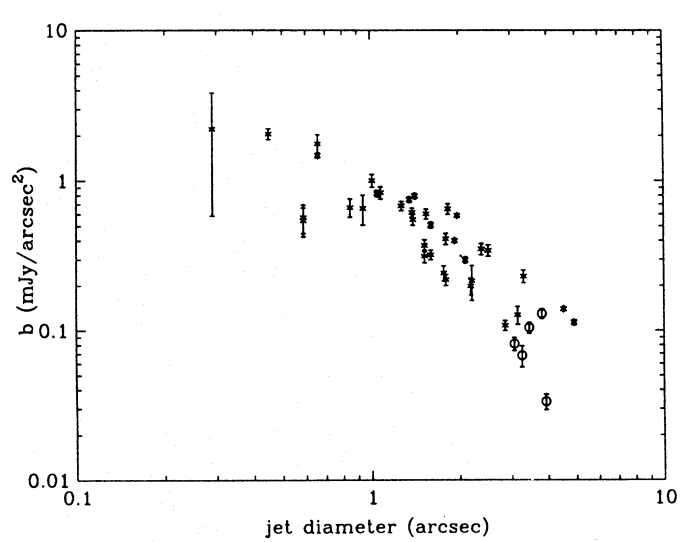


Fig. 8b. The deconvolved jet brightness of B2 0844+31, at 4885 MHz, plotted against deconvolved transverse jet size. Open circles refer to the counter-jet

In 0844+31 spectral index variations are seen in both lobes. The bright outer ridges of emission have spectral indices \sim 0.8–0.9 in the south lobe and \sim 1.0 in the Northern one. The lower brightness regions have steeper spectra (\sim 1.6–1.8).

In 1521+28 spectral gradients are marginal, if any, in the northern lobe, while the southern lobe shows a clear trend: the spectral index is (\sim 0.6) around the hot spot, and it steepens up to (\sim 1.0) far from it. Furthermore the spectrum is steeper than average on the western edge of the lobe.

6.3. Polarization

The lobes are significantly polarized at 6 cm and somewhat less at 20 cm. Figures 12, 13 and 14 display the low resolution maps with the E vectors superimposed. The comparison at the two frequencies is made by means of the 10" resolution maps and only where the total and polarized intensities are at least 5 times the r.m.s. noise level.

In 0844+31 the northern lobe is more polarized than the southern one at both frequencies (15% against 12.5% at 5 GHz;

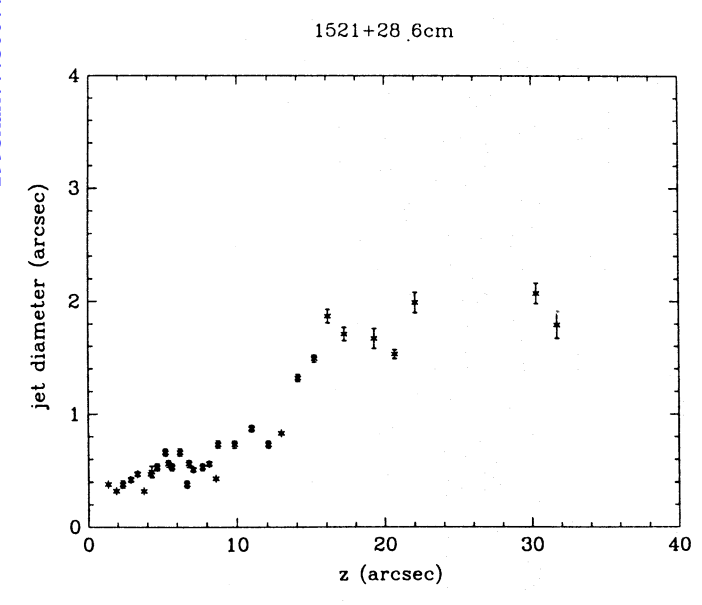


Fig. 9a. The deconvolved FWHM jet diameter of B2 1521+28, plotted against angular distance from the core

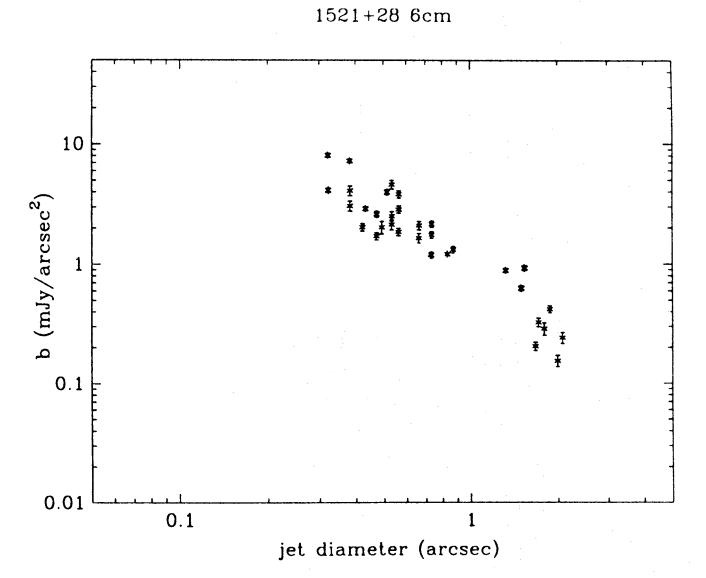


Fig. 9b. The deconvolved jet brightness of B2 1521+28, at 4885 MHz, plotted against deconvolved transverse jet size

13% against 7.1% at 1.4 GHz). The northern lobe is also less depolarized than the southern one, as found also for the hot spots. In the north lobe the depolarization ratio is $\sim 0.76 \pm 0.05$ while in the south it is $\sim 0.64 \pm 0.05$. The integrated rotation measure is $\sim -47 \, \mathrm{rad} \, \mathrm{m}^{-2}$. Variations of R.M. are seen in both lobes; within $\pm 20 \, \mathrm{rad} \, \mathrm{m}^{-2}$ in the northern one; larger (from -10 to $-50 \, \mathrm{rad} \, \mathrm{m}^{-2}$) in the southern one.

In 0836+29 the polarization map at 1.4 GHz is of poor quality, and polarization is clearly detected only in a few brighter points. At 5 Ghz polarization is detected in both lobes. Due to the low quality the 1.4 GHz polarization map, the study of the depolarization is possible only in the brighter areas. The R.M.,

Table 6. Expansion regimes

Object	Distance (kpc)	$\mathrm{d} heta/\mathrm{d}z$
0836+29	0–13 13–22 22–32 35–55	~ 0.1 ~ 0.0 ~ 0.12 ~ 0.0
0844+31	0–15 15–35 > 35	~ 0.1 ~ 0.0 ~ 0.2
1521+28	0-4 4-12 12-19 > 20	~ 0.1 ~ 0.04 ~ 0.20 ~ 0.0

0844+31 jet 5"

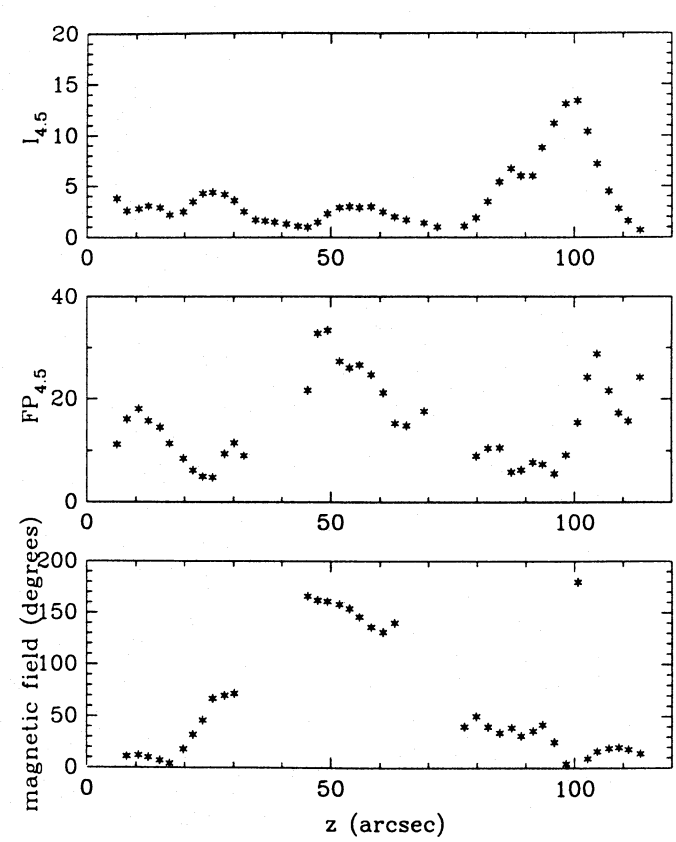


Fig. 10. Profiles of: total intensity (top), fractional polarization (center) and magnetic field orientation (bottom), along the ridge line of the northern (main) jet, at 4885 MHz

measured in correspondence to the southern hot spot, is ~ 15 rad m⁻².

In 1521+28 the polarization at 5 GHz is similar in both lobes. The depolarization ratio is $\sim 0.29 \pm 0.05$ in the northern lobe and $\sim 0.74 \pm 0.05$ in the southern one. The integrated rotation measure is $\sim 9 \deg m^{-2}$. Variations around this value across the lobes are minor ($\lesssim \pm 10 \, \text{rad m}^{-2}$).

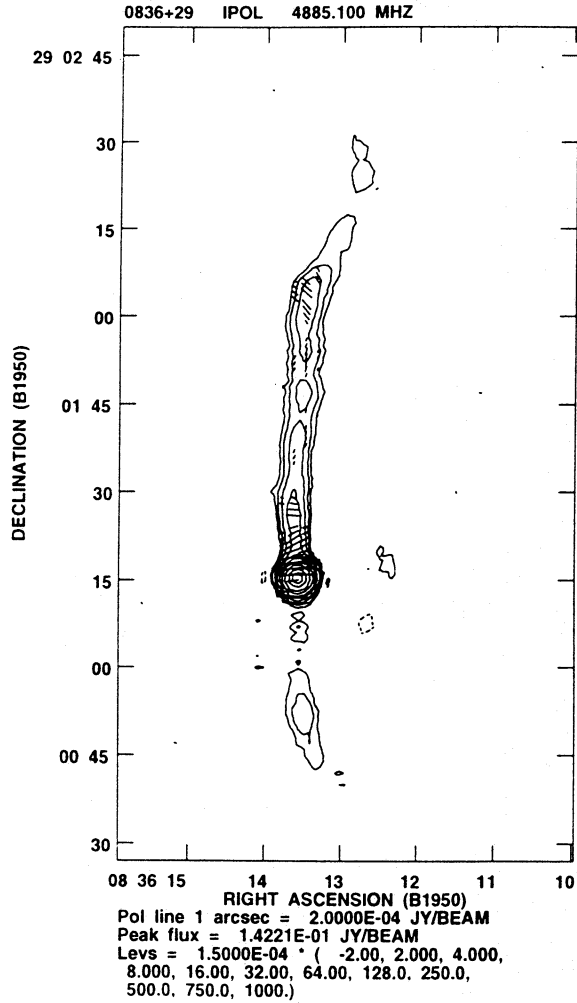


Fig. 11a. Linear polarization vector distribution, at 4885 MHz, for the jet of B2 0836+29 superposed on total intensity map at resolution of 3.3". The magnetic fied orientation is obtained by 90 deg. rotation

In all three sources the intrinsic electric vector p.a. is close ($\lesssim 15$ deg.) to that measured at 5 GHz. By applying the small corrections required one obtains the magnetic field geometry across the sources. The structure of the magnetic field in the lobes of 0844+31 and in the northern lobe of 1521+28 appears mostly circumferential, as found in several other sources (Bridle et al. 1991). In the southern tail of 0836+29 and in the southern lobe of 1521+28 the field is aligned with the radio axis.

7. Discussion

7.1. Physical parameters of the sources

The equipartition internal energy, energy density and magnetic field have been computed with standard formulae (Pacholczyk 1970). We assumed an ellipsoidal geometry for the lobes and a cylindrical geometry for the jets, filling factor 1 and equal energy in relativistic electrons and protons. The computed values are given in Table 10.

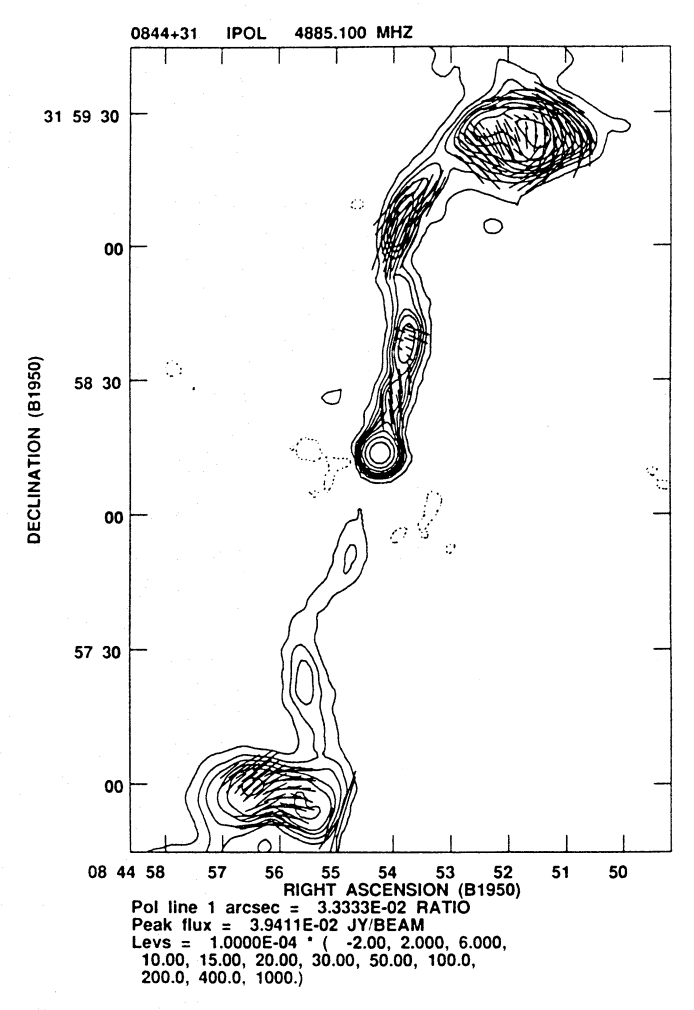


Fig. 11b. Magnetic field orientation for the jet of B2 0844+31, after correction for Faraday rotation

Table 7. Jet properties

	0836+29	0844+31	1521+28
Main jet	North	North	South
$S_{20\mathrm{cm}} \ S_{\mathrm{mj}}/S_{\mathrm{t}}$	50 mJy ∼ 0.08	75 mJy ∼ 0.06	≥ 30
$S_{ m mj}/S_{ m c}$	~ 0.45	~ 2.5	~ 2.0
$d\theta/dz$	~ 0.1	~ 0.1	~ 0.1
δ	~ 1.5	~ 1.7	~ 1.6
% pol.(6 cm)	11.5	14.7	22
Rot. measure	60	-55/-80	-13/+7
Counter jet	South	South	North
$\overline{S_{20 ext{cm}}}$	7 mJy	39 mJy	3 mJy
$S_{ m mj}/S_{ m t}$	0.01	0.03	

7.2. Spectral properties and source life times

The spectral variations seen in the lobes of the three sources are interpreted as being due to energy losses, for synchrotron and

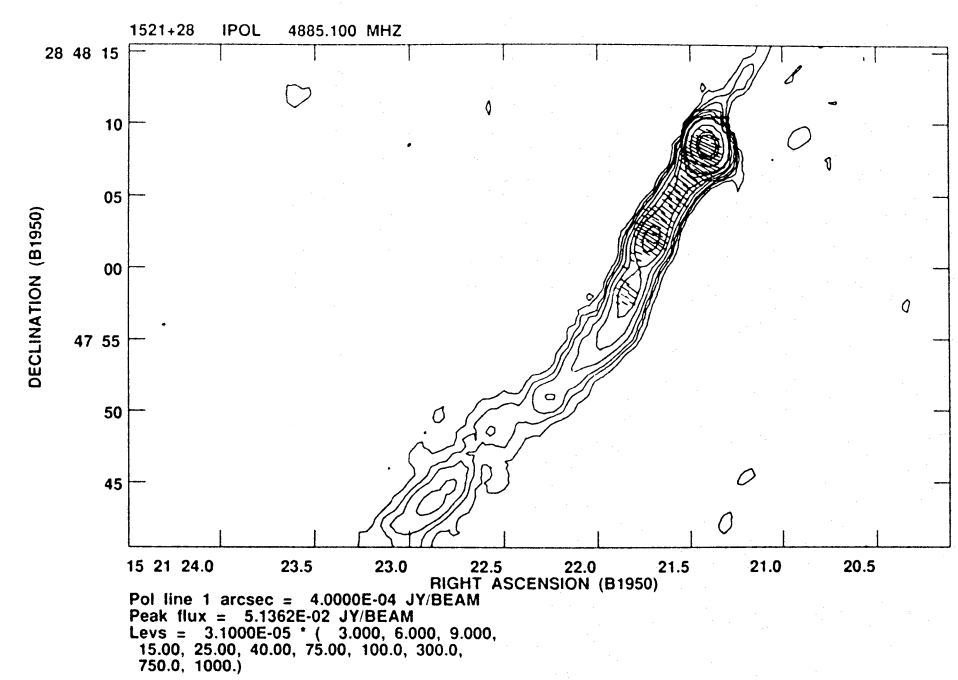


Fig. 11c. Linear polarization vector distribution, at 4885 MHz, for the jet of B2 1521+28 superposed on total intensity map at resolution of 1.6". The magnetic field orientation is obtained by 90 deg, rotation

Table 8. Hot spot properties

	0836+29	0844+31	1521+28
Northern hot spot			
S (6 cm) (mJy)		65	
Size (kpc)		13 x 10	
Spectral index		0.67	
% pol. (6 cm)		34	
Southern hot spot			
S (6 cm) mJy	29	38	5
Size (kpc)	14 x 8	10 x 8	5 x 1
Spectral index	0.55	0.83	0.5
% pol. (6 cm)	40	28	50
% pol. (6 cm)	40	28	50

Inverse Compton, of the relativistic electrons of different ages. We assume for the magnetic field the equipartition values (see Table 10).

With these values the synchrotron losses are comparable to the I.C. losses, and the computed electrons lifetimes are close to the maximum possible value.

We take the source ages as corresponding to the larger values of the electrons lifetimes, which are derived from the larger believable values of the spectral index. Application of the Jaffe-Perola model (Jaffe & Perola 1973) gives ages $\cong 4-7 \ 10^7$ years.

The average energy supply (F_e) from the nucleus (see Sect. 7.7), required to feed the lobes in their life times (Table 11), are $\sim 2 \cdot 10^{43}$ erg s⁻¹, about 100 times the total radio luminosity.

The average advance velocity of the lobes is $\sim 4 \cdot 10^8$ cm s⁻¹.

Table 9. Lobe properties

	0836+29	0844+31	1521+28
North Lobe			
$S_{20\mathrm{cm}}$ (mJy)	269	406	173
$\theta_1 \times \theta_2$ (arcsec)	70×60	148×92	56×52
$d_1 \times d_2$ (kpc)	83×71	150×93	59×55
% pol. (6 cm)	18	20	18
D^{a}	-	0.76	0.28
Rot. meas. $(rad m^{-2})$	-	- 47	9
α	1.04	1.06	0.92
South Lobe			
$S_{20\mathrm{cm}}$ (mJy)	265	358	332
$\theta_1 \times \theta_2$ (arcsec)	184×25	120×110	96×60
$d_1 \times d_2$ (kpc)	218×30 122×111	101×60	
% pol.	34	13	23
$D^{\hat{\mathbf{a}}}$	-	0.64	0.74
Rot. meas. $(rad m^{-2})$	15	- 47	9
α	0.82	0.96	0.71

^a D is the depolarization ratio.

7.3. The jet flavour

The jets in all three sources are characterized by a small opening angle and the presence of several brightness knots. The brightness, as a function of jet size, shows a clear sub-adiabatic behaviour.

The first two characteristics recall one of the two "jet flavours" described by Bridle (1986), generally interpreted in terms of strong supersonic flow. The sub-adiabatic behaviour of the brightness seems better explained in terms of reacceleration of the electrons in correspondence of shocks, which manifest

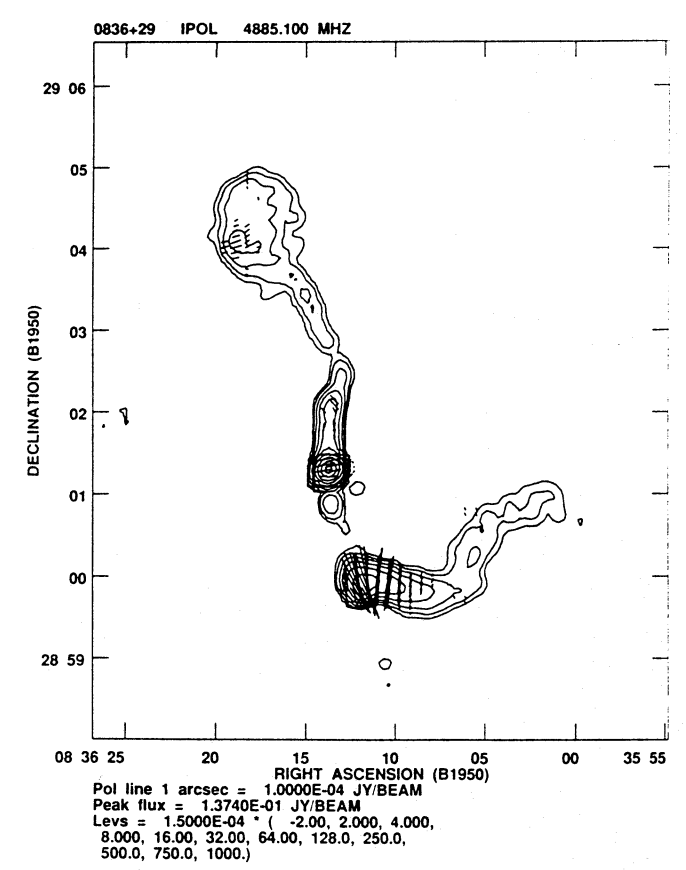


Fig. 12. Linear polarization vector distribution, at 4885 MHz, for B2 0836+29, superposed on total intensity map at resolution of 10.9". The magnetic field orientation is obtained by 90 deg. rotation

themselves as brightness knots, rather than in terms of low Mach number turbulent entraining jets (Bicknell 1986a).

The modest prominence of the hot spots suggests, however, that the Mach number cannot be very high at the end of the jet.

7.4. Jet confinement

We have seen that the jets expand at a variable rate. The growth of the jet transverse size is similar in all three sources: a regime of expansion is followed by a collimation "shoulder" where $\mathrm{d}\theta/\mathrm{d}z\sim0$, then re-expansion.

Steady free jets are expected to expand at a constant rate and this is clearly not observed.

We might expect that the jets are freely expanding at the beginning and then become confined.

The minimum pressures required to confine the jets can be estimated from the equipartion calculations (see Table 10). Figures 15a,b,c show the minimum pressure as a function of distance from the core. Thermal pressures of the necessary magnitude could be provided by an external medium at $T \sim$ few $10^7 \, \text{K}$ and densities $\sim 0.1-0.002 \, \text{cm}^{-3}$ over the range of distances from the core. These parameters are similar to those of gaseous X-ray halos around several nearby ellipticals (Forman et al. 1985).

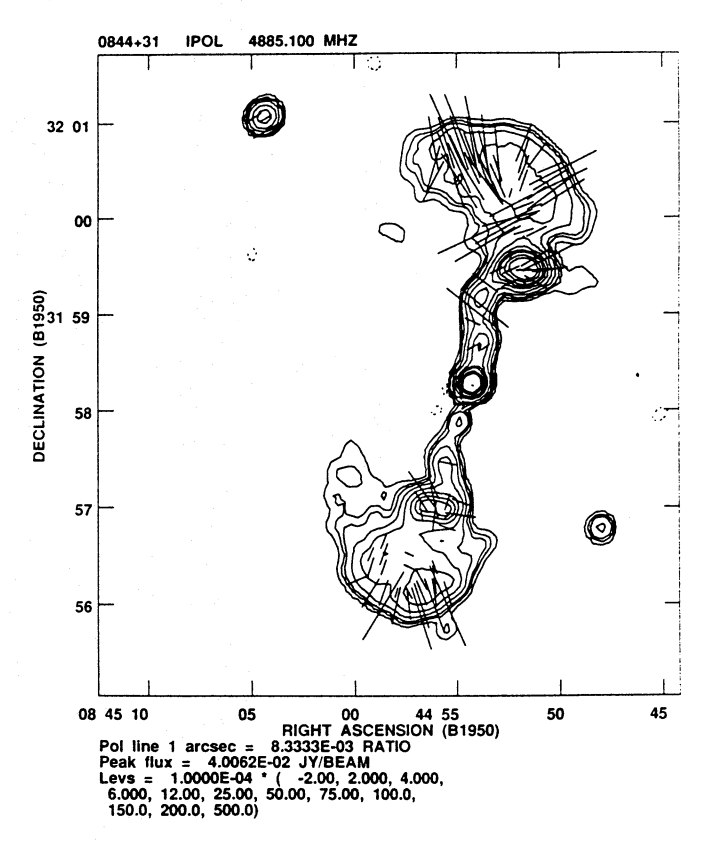


Fig. 13. Linear polarization vector distribution, at 4885 MHz, for B2 0844+31, superposed on total intensity map at resolution of 10.6". The magnetic field orientation is obtained by 90 deg. rotation

From two of the sources, 0836+29 and 0844+31, X ray emission has been reported from the Einstein Observatory (Morganti et al. 1988). In the case of 0844+31 the X ray counts are too few to say if the emission is extended or if it is unresolved and so due to nuclear emission. In the case of 0836+29, the X ray emission is extended and clearly associated to the cluster Abell 690, of which our galaxy is the brighter member. The jets lie within the high brightness X-ray region, while both southern and northern radio lobes are at the edge of the X-ray emission. The jet minimum pressure at $\sim 10\,\mathrm{kpc}$ seems higher by a factor 5 than the estimated value of the external pressure, while at larger distances the two pressures are comparable. This may be taken as an indication that the jets initially expand freely and than become confined by the external gas pressure.

7.5. Source orientation

In spite of their relatively large sizes, we argue that the three sources are oriented at moderate angles with respect to the line of sight. The first argument is based on the large jet to counterjet brightness ratio, which may be easily interpreted in terms of Doppler beaming from relativistic jets. The asymmetry will be used in a next section to estimate the jet velocities.

A further argument is based on the relative core strength. In all three sources the core intensity, relative to the extended emission, is larger than the average for sources of that total radio

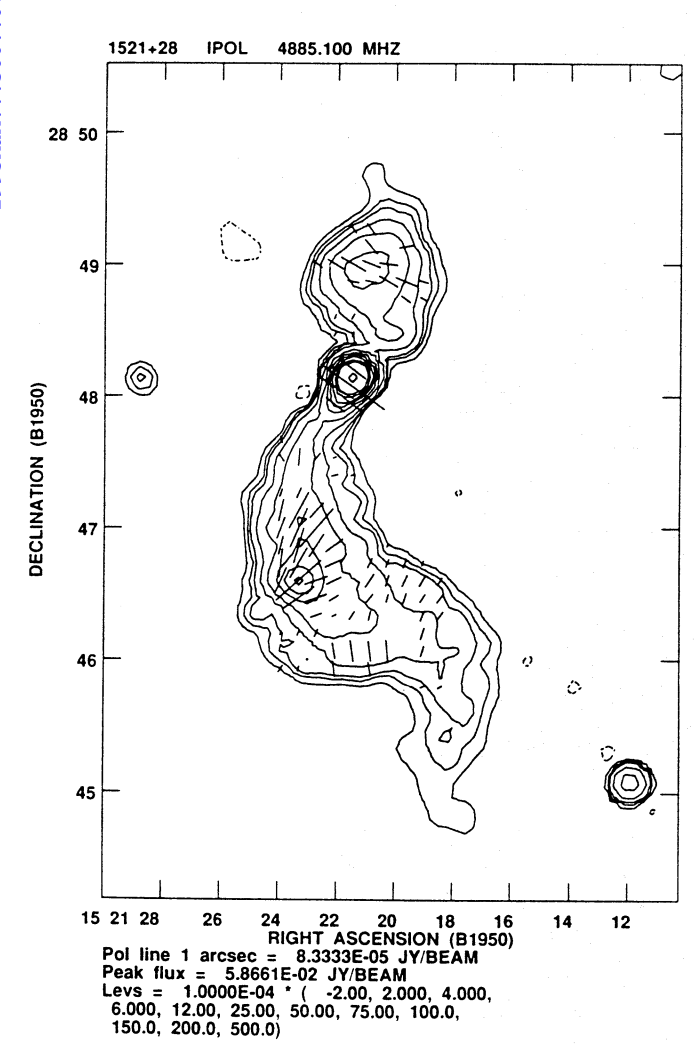


Fig. 14. Linear polarization vector distribution, at 4885 MHz, for B2 1521+28, superposed on total intensity map at resolution of 10.9". The magnetic field orientation is obtained by 90 deg. rotation

luminosity (see Sect. 3). If we assume that the cores represent the base of a two sided intrinsically symmetric relativistic jet, their apparent luminosity will be strongly dependent on the viewing angle. The parameter $P_{\rm cn}$, defined in Sect. 3, can be used as an orientation indicator. If radiogalaxies of a given total radio power are randomly oriented with respect to the line of sight, it is easy to find that, for $\theta < 50$ deg.,

$$P_{\rm cn} \sim \frac{\left(1-eta_{
m j}/2
ight)^{(2+lpha)}}{(1-eta_{
m j}\cos heta)^{(2+lpha)}} \; .$$

We expect $P_{\rm cn} < 1$ for sources at angles larger than 60 deg. and $P_{\rm cn} > 1$ for angles smaller than 60 deg. The three sources have $P_{\rm cn}$ values ranging from 1.8 for 0844+31 up to 10 for 0836+29. If $P_{\rm cn}$ values larger than 1 are due to Doppler effects only, from the above formula, the viewing angles have to be less than 31, 51 and 37 deg. for 0836+29, 0844+31 and 1521+28 respectively. The limit is not very strong for 0844+31, but is more tight for the other two sources. Of course any intrinsic dispersion in the core luminosities or variability effects would weaken these limits.

Table 10. Equipartition parameters

	0836+29	0844+31	1521+28
Main jet			
at 5 kpc			
$u_{\rm eq} (10^{-11} {\rm erg cm^{-3}})$	7	7.5	7
$H_{ m eq} \left(\mu { m G} ight)$	28	28	28
at 30 kpc			
$u_{\rm eq} (10^{-11} {\rm erg cm^{-3}})$	1.1	1.1	1.0
$H_{ m eq}$ ($\mu m G$)	11	11	10
Hot spots			
$u_{\rm eq} (10^{-11} {\rm erg cm^{-3}})$	-	1 (N)	-
$u_{\rm eq} (10^{-11} {\rm erg cm^{-3}})$	1 (S)	0.5 (S)	1.8 (S)
$H_{ m eq}~\mu{ m G}$	-	11 (N)	_
$H_{ m eq}~\mu{ m G}$	11 (S)	8 (S)	15 (S)
Lobes			
$U_{\rm eq}~(10^{58}~{\rm erg})$	1.1	2.0	1.4
$u_{\rm eq} (10^{-12} {\rm erg cm^{-3}})$	1.1	0.6	0.8
$H_{\mathrm{eq}}~(\mu\mathrm{G})$	3.6	2.4	3.0

Table 11. Ages and power supply to the lobes

	0836+29	0844+31	1521+28
ν _{break} (GHz)	4.0	2.4	4.7
$T_{\rm s}(10^7 { m y})$	3.8	5–6	4.2
$F_{\rm e}$ (erg/s)	1.8 10 ⁴³	2.4 10 ⁴³	$2.2 \ 10^{43}$

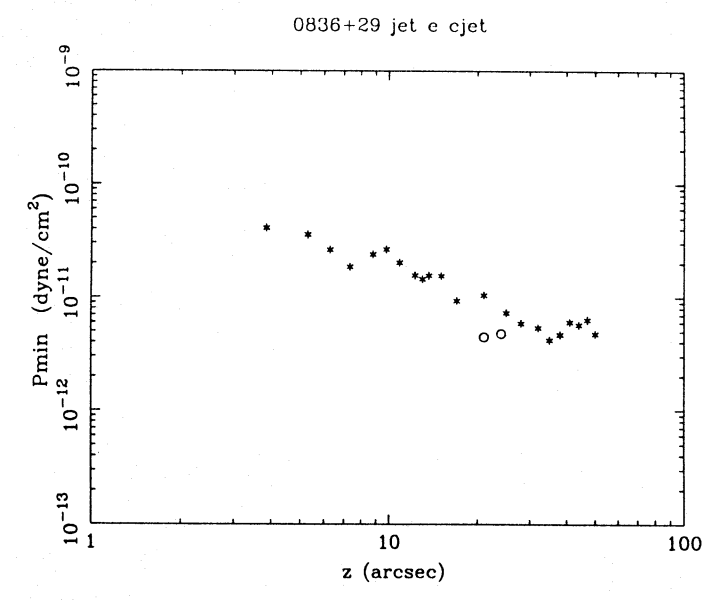


Fig. 15a. Plot of internal minimum pressure of the jets of B2 0836+29 against distance from the radio core. Open circles refer to the counterjet

Instead of taking a viewing angle for each source, we take an average upper limit for the three all together, of 45 deg.

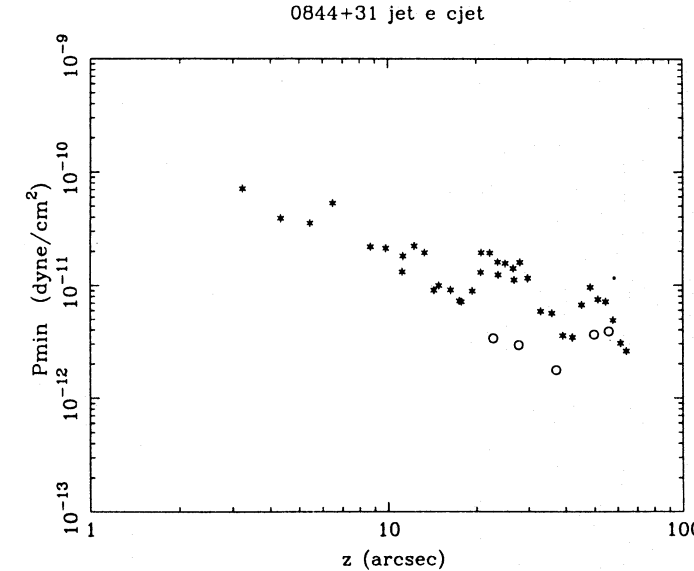


Fig. 15b. Plot of internal minimum pressure of the jets of B2 0844+31 against distance from the radio core. Open circles refer to the counterjet

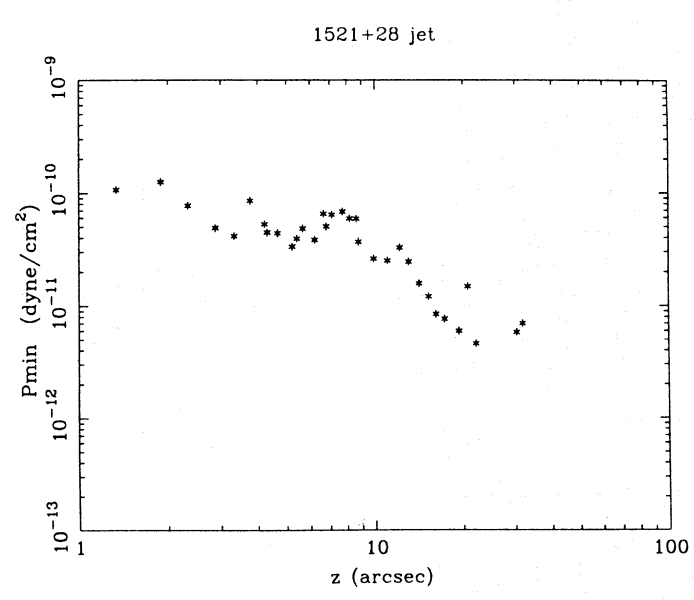


Fig. 15c. Plot of internal minimum pressure of the jet of B2 1521+28 against distance from the radio core

Another argument for a moderate inclination is that two of the sources, 0844+31 and 1521+28, display a clear Laing-Garrington effect (Laing 1988; Garrington et al. 1988), namely the lobe on the side of the main jet is less depolarized than the other lobe. This depolarization is generally attributed to propagation of the radiation through paths of different length across a magneto-active dishomogeneous medium. Significant path length differences, and therefore source axis at small angles to the line of sight, are required. It has to be noted, however, that in the case of 1521+28, where the depolarization asymmetry is stronger, the source is also asymmetric in lobe-length, so that

it could be suggested instead that it displays the Pedelty et al. asymmetry (Pedelty 1989), which is attibuted to density asymmetry in the ambient medium. This weakens the depolarization asymmetry as an argument for orientation close to the line of sight.

We also suggest a lower limit ~ 25 deg. to the orientation angle, in order not to have too large intrinsic dimensions for the three sources, whose projected sizes are already larger (by at least 50%) of the average size of sources of similar radio power.

Concluding, the suggested plausible range of orientation angles is $\sim 25-45$ deg.

7.6. Velocity of the jets

We have shown, in Sect. 4.2, that in all three sources the jets are very asymmetric in brightness. The jets asymmetry is strong in the first 10 kpc and then reduces at larger distances. Following the scenario recently presented by Laing (1994) and Bicknell (1994), (see also Parma et al. 1994) we assume that the jets are relativistic up to $\sim 5{-}10\,\mathrm{kpc}$ from the core, so as to explain the strong brightness asymmetry in terms of Doppler favoritism, and then are decelerated to lower velocities, possibly by entrainment of external gas.

Assuming that the jets are intrinsically symmetric, we can derive, from the observed brightness asymmetry, A_j , the quantity

$$\beta_{j} \cos \theta = \left(A_{j}^{\frac{1}{2+a}} - 1\right) \left(A_{j}^{\frac{1}{2+a}} + 1\right)^{-1}.$$

At a distance of 5 kpc from the core, we have

 $\begin{array}{ccccc} 0836+29 & A_{\rm j} > 10 & \beta_{\rm j} \, \cos\theta > 0.4 \\ 0844+31 & A_{\rm j} > 30 & \beta_{\rm j} \, \cos\theta > 0.6 \\ 1521+28 & A_{\rm j} \gtrsim 15 & \beta_{\rm j} \, \cos\theta \gtrsim 0.5 \end{array}$

The minimum values of β_j are, of course, obtained for $\theta=0$. If we assume as plausible range $25<\theta<45$ deg., the jets velocity at ~ 5 kpc from the core would range from ~ 0.5 to 0.85c.

At larger distances from the core, e.g. at 30 kpc for 0836+29 and 0844+31, and at 20 kpc for 1521+28 (this is the the counterjet length), the jets asymmetry is smaller and implies values of $\beta_{\rm j} \cos\theta \sim 0.2$, lower by a factor 2 to 4 than the corresponding ones at 5 kpc.

7.7. The energy budget and the Mach number of the jet

An often used argument to estimate the jet velocities is the energy budget (see Bicknell 1986b). It is assumed that the flux along the jet has supplied the energy accumulated in the radio lobes plus the energy radiated during the source lifetime, plus the work done in the lobe expansion. In most cases, as here, the first term overwhelms the second one and is comparable to the third. With the usual assumption of energy equipartition between relativistic particles and magnetic field, and neglecting thermal energy, the energy flux along the jet, $F_{\rm e41}$, in units of $10^{41}~{\rm ergs\,s^{-1}}$, is given by:

$$F_{\rm e41} \sim 7.8 \ v_{\rm j8} \ r_{\rm j,kpc}^2 \ p_{\rm j-10} \ (1 + bM_{\rm j}^2)$$

(Bridle et al. 1991) where $r_{\rm j}$ is the jet radius (we use the "top hat" approximation, with $r_{\rm j}^2 \sim \phi^2/3$, where ϕ is the transverse HWHM of the jet), p_{j-10} the minimum (equipartition) pressure in the jet in units of 10^{-10} dyn cm⁻², v_{j8} the velocity in the jet in units of 10^8 cm s⁻¹, $M_{\rm j}$ the jet Mach number and $b \sim 1/4$.

It is assumed that the jet is in pressure equilibrium with the external medium. We take

$$F_{\rm e} = 2 U_l/T_{\rm rs}$$
,

where the factor 2 accounts for the expansion work. The energy budget relation, together with the values of $\beta_j \cos \theta$ deduced from the initial jet asymmetry, and taking the range of orientations of 25–45 deg, allows to evaluate M_j . In doing this we must correct the jet brightness, used to compute p_j , for the Doppler brightening. The corrections are of the order of a factor 2–3.

We find that $M_{\rm j}$ is in the range from 3.5 to 5.5. The formal errors are $\sim 30\%$ on $\beta_{\rm j}$ $(1 + bM_{\rm j}^2)$, and ± 1 on $M_{\rm j}$.

7.8. Jet oscillations

The lateral oscillations of the jets, described in Sect. 4.4, can be ascribed to various causes. These include orbital or precessional motion and growing Kelvin-Helmoltz instabilities in the jet boundary.

Orbital motion alone should produce a single oscillation wavelength with fixed amplitude and mirror symmetry of the jets with respect to the nucleus. The source 0844+31 seems to posses these characteristics, but to our knowledge, no companion is present to cause an orbital motion. At the same time the mirror symmetry of the jets of 0844+31 excludes the precessional model, which would imply anti-symmetry of the jets.

Interpreting the transverse oscillations as a result of Kelvin-Helmoltz instabilities on a confined jet is attractive in that it allows to explore the range of Mach number consistent with it. We use the relation of Hardee (1987), which expresses the oscillation wavelength as a function of the jet Mach number, $M_{\rm j}$, and the ratio, η , between the densities in the jet and in the external medium. The relation is

$$\lambda \sim \frac{5.2 \ M_{\rm j} R_{\rm j}}{0.66 + \eta^{0.5}}$$

and is reasonably correct for $M_{\rm j}\gtrsim 3$. The minimum $M_{\rm j}$ is obtained for $\eta=0$ and is given by

$$M_{\rm j} = 0.13 \frac{\lambda}{R_{\rm j}} \ .$$

Using the ratios λ/R_i reported in Sect. 4.4, we obtain

0836+29
$$M_{\rm j} \sim 3.3$$

0844+31 $M_{\rm j} \sim 7.8$
1521+28 $M_{\rm j} \sim 3.6$.

The above values are not inconsistent with the estimates of the previous section.

7.9. The hot spots

The hot spots seen in these three sources, have some peculiarity. In two cases they are embedded in the lobes. In this sense they differ from the classical hot spots of FRII radiosources, where the hot spots are generally located in the outer parts of the radio lobes. A kind of similarity may be found with the hot spots in WAT sources, where the jet flaring is followed by a less collimated forward flow. The similarity is particularly strong in the case of 0836+29.

Alternatively, for 0844+31 and 1521+28, one could think to precession of the central engine (as in Cox et al. 1991). The presently observed hot spots would be the impact point of the jet, while the radio plasma more far away would be the result of backflow from previous hot spots located at different further positions, which have now faded.

8. Conclusions

We have studied three sources of intermediate radio luminosity at two frequencies and several resolutions, with the VLA.

The sources show properties which are intermediate between the FRII and the FRI.

- (a) They are characterised by bright one sided jets with small opening angles. The jet asymmetry is large close to the core (< 10 kpc) and reduces gradually at larger distances.
- (b) The radio cores are more prominent, with respect to the extended component, than the average of radio galaxies of similar radio luminosity.
- (c) Two of the sources show clearly the Laing-Garrington effect, namely the lobe on the side of the main jet is less depolarized than the other lobe.
- (d) The hot spots tend to be located in the inner regions of the lobes, contrary to what mostly found in typical FRII sources.
- (e) Based on a), b) and c), we suggest that these sources are oriented at moderate angles to the line of sight ($25 < \theta < 45$ deg.).
- (f) On the basis of the jet asymmetry and of the energy budget we estimate the jet velocity and Mach number. We conclude that the jets are mildly relativistic at < 5 kpc, with $\beta_{\rm j} \sim$ 0.6–0.8, but their velocity reduces to \lesssim 0.2c at distances \gtrsim 20 kpc. The jet Mach numbers are estimated in the range 4–6.

Acknowledgements. We thank R. Primavera for the photographic reproduction of the figures. A. Capetti wishes to acknowledge partial financial support and the hospitality received from the N.R.A.O. The National Radio Astronomy Observatory is operated by Associated Universities, Inc., under contract with the National Science Foundation.

References

Baars J.W.M., Genzel R., Pauliny-Toth I.I.K., Witzel A., 1977, A&AS 61, 99

Bicknell G.V., 1986a, ApJ 305, 109 Bicknell G.V., 1986b, ApJ 300, 591 Bicknell G.V., 1994, in: Bicknell G.V., Dopita M.A., Quinn P.J. (eds.)The First Stromlo Symposium: The Physics of Active Galaxies, p. 231

Bridle A.H., 1986, Can.JPh., 64, 353

Bridle A.H., Baum S.A., Fomalont E.B., et al., 1991, A&A 245, 371 Clark B.G., 1980, A&A 89, 377

Cox C.I., Gull S.F., Scheuer P.A.G., 1991, MNRAS 252, 558 de Ruiter H.R., Parma P., Fanti C., Fanti R. 1990, A&A 227, 351 de Ruiter H.R., Capetti S., Morganti R., et al., 1993, in: Roser H.J., Meisenheimer, (eds.) Jets in Extragalactic Radio Sources, p. 21

Fanti R., Lari C., Parma P., et al., 1982, A&A 110, 169

Fanti C., Fanti R., de Ruiter H.R., Parma P. 1987, A&AS, 69, 57 Forman W., Jones C., Tucker W., 1985, ApJ 293, 102

Garrington S.T., Leahy J.P., Conway R.G., Laing R.A., 1988, Nat 331, 147

Garrington S.T., Conway R.G., Leahy J.P., 1991, MNRAS 250, 171 Hardee P.E., 1987, ApJ 313, 607 Hogbom J., 1974, ApJS 15, 417 Jaffe W.J., Perola G.C., 1973, A&A 26, 423

Laing R.A., 1988, Nat 331, 149

Laing R.A, 1994, in: The First Stromlo Symposium: The Physics of Active Galaxies, Bicknell G.V., Dopita M.A., Quinn P.J., (eds.). p. 227

Morganti R., Fanti R., Gioia I.M., et al., 1988, A&A 189, 11

Napier P.J., Thompson A.R., Ekers R.D., 1983, IEEE 71, 1295

Parma P., Fanti C., Fanti R., Morganti R., de Ruiter H.R 1987, A&A 181, 244

Parma P., de Ruiter H.R., Fanti R., Laing R., 1994, in: Bicknell G.V.,
Dopita M.A., Quinn P.J. (eds.) The First Stromlo Symposium: The
Physics of Active Galaxies, p. 241

Pedelty J.A., Rudnick L., McCarthy P.J., Spinrad H., 1989, AJ 97, 647 Schwab F.R., 1980, Proc. SPIE 231, 18

Venturi T., Castaldini C., Feretti L., et al., 1994, in: Zensus J.A., Kellerman K.I. (eds.) Compact Extragalactic Radio Sources NRAO Proceedings Series, p. 67